Journal of The Electrochemical Society, **152** (1) A88-A92 (2005)
0013-4651/2004/152(1)/A88/5/$7.00 © The Electrochemical Society, Inc.

Preparation and Electrochemical Characterization of Perovskite/YSZ Ceramic Films

2.190

Daniel Z. de Florio,[a] Reginaldo Muccillo,[a,*] Vincenzo Esposito,[b,] Elisabetta Di Bartolomeo,[b] and Enrico Traversa[b,*,z]**

[a]*Centro Multidisciplinar para o Desenvolvimento de Materiais Cerâmicos, CCTM-Instituto de Pesquisas Energéticas e Nucleares, S. Paulo, SP, Brazil 05422-970*
[b]*Dipartimento di Scienze e Tecnologie Chimiche, Università di Roma "Tor Vergata," 00133, Roma, Italy*

Perovskite-type $La_{0.8}Sr_{0.2}Co_{0.8}Fe_{0.2}O_{3-\delta}$ powders were prepared using a complex polymeric precursor method. Thermal analysis was carried out on the perovskite precursor to investigate the oxide-phase formation. The structural phase of the powders was determined by X-ray diffraction. These results showed that the decomposition of the precursors occurs in a two-step reaction and temperatures higher that 1000°C are required for these decomposition reactions. For the electrochemical characterization, $La_{0.8}Sr_{0.2}Co_{0.8}Fe_{0.2}O_{3-\delta}$ electrodes were deposited by a wet spray technique on dense yttria-stabilized zirconia (YSZ) layers. The morphology of the deposited perovskite thick films (~50 μm) was investigated by field emission scanning electron microscopy and showed a porous microstructure. Electrochemical impedance spectroscopy (EIS) measurements were carried out under synthetic air flux at temperatures ranging from 200-600°C in the 10 mHz-10 MHz frequency range showing an interfacial electrical resistance related to the $La_{0.8}Sr_{0.2}Co_{0.8}Fe_{0.2}O_{3-\delta}$ electrodes. EIS measurements were also performed in the same frequency range at different oxygen partial pressures (10^{-5}-1 atm) at 600°C. At this temperature and frequencies below 0.1 MHz, the electrical response to the applied signal of the electrode material is best fitted by two semicircles, which can be related to charge-transfer processes. The activation energy for the limiting step (adsorption/desorption) was found to be 1.6 eV.
 [DOI: 10.1149/1.1824043]

Manuscript submitted December 29, 2003; revised manuscript received June 1, 2004. Available electronically December 1, 2004.

Mixed ionic and electronic conductors (MIECs) have been widely studied for applications as electrodes in solid oxide fuel cells (SOFCs)[1] and in non-Nernstian electrochemical sensors.[2] $La_{0.8}Sr_{0.2}Co_{0.8}Fe_{0.2}O_{3-\delta}$ (LSCF) is one of the most promising cathode materials for SOFC at intermediate temperatures because of its higher oxygen ion conductivity and higher tolerance towards Cr species compared to LSM ($La_xSr_{1-x}MnO_{3-\delta}$) electrodes.[3-5] The interfacial polarization that occurs at the electrolyte interface affects strongly the SOFC performance, and is directly related to the electrical resistance associated with each cell component. The rate of charge transfer is also known to be a function of microstructural properties of the electrocatalyst such as particle size and surface area. Hence, it is important to understand the behavior of electrodes in terms of microstructural and electrochemical parameters to optimize the SOFC performance.[4]

For this reason, control of grain size and of microstructure can be achieved through chemical synthesis of the cathode materials. The increase in the triple-phase boundary (TPB) length results in a decrease in polarization drops and in an improved performance of cathode materials. TPB can be increased with perovskite-type oxides with nanometric grain size. On the other hand, better performance of non-Nernstian electrochemical sensors was observed when nanometer electrodes were used as sensing electrodes.[2] The electrochemical impedance spectroscopy (EIS) technique is a widely used tool for studying the electrical characterization of SOFC. EIS allows the separation, in the frequency domain, of each contribution to the total resistance of the cell.[5]

Experimental

Powder preparation.—The LSCF powders used in this study were prepared using a complex polymeric precursor method.[6] The metal nitrates $La(NO_3)_3 \cdot 6H_2O$ (99.99%, Aldrich), $Sr(NO_3)_2$ (99%, Aldrich), $Fe(NO_3)_3 \cdot 9H_2O$ (98%, Aldrich), and $Co(NO_3)_2 \cdot 6H_2O$ (99%, Carlo Erba) were used in stoichiometric proportion to obtain the final LSCF powders. The nitrates were dissolved separately in ethylene glycol (99.5%, Carlo Erba) in a ratio of 40 mL of ethylene glycol to 10 g of metal salts. These solutions were mixed together and a citric acid (99.5%, Carlo Erba) with ethylene glycol (60/40 wt %) solution was added to complex the metal ions in the molar proportion of 1.8. The obtained solution was stirred for 1 h at room temperature; then it was heated on a hot plate under stirring until a viscous dark red gel was formed, as a result of the evaporation and the polyesterification. This gel was dried overnight at 100°C, fired at 200°C for 15 h, and then calcined at 600°C for 6 h to remove any remaining organic material. The resulting product was milled in isopropanol for 12 h and calcined again with a heating rate of 5°C/min at 800°C or at 1100°C for 5 h in air. All samples were furnace-cooled to room temperature. Simultaneous thermogravimetric-differential thermal analysis (TG-DTA, Netzsch STA 409) of the hygroscopic hydrated nitrates and of the perovskite precursor gel was carried out to calculate the amount of constituient water molecules and to investigate the oxide-phase formation, respectively. The structural characterization of the perovskite powder was performed by X-ray diffraction (XRD) analysis (Philips X'Pert) with Cu Kα radiation, in the $10° \leq 2\theta \leq 95°$ range.

Film deposition.—The perovskite electrodes were fabricated by a wet spray technique.[7-9] The LSCF powder calcined at 1100°C was ballmilled using an agate ball mortar and mixed with 10 wt % polyvinyl butyral-co-vinyl alcohol-co-vinyl acetate (Aldrich) binder to form a suspension dispersed in tetrahydrofuran. The suspension was sprayed on a tape-cast yttria-stabilized zirconia (YSZ) substrate using nitrogen as the gas carrier, over an approximately 0.2 cm^2 area. The binder used is soluble in tetrahydrofuran and forms a film surrounding the perovskite particles preventing their agglomeration as the solvent evaporates during the deposition. The final result was a porous network of perovskite particles tied by the binder.[8,9] Current collectors were attached to the deposited electrodes using gold wires and platinum paste. The as-prepared samples were sintered at 800°C for 1 h with heating and cooling rates of 5°C/min. The morphology of the deposited thick electrode films (~50 μm) was investigated using a field emission scanning electron microscope (FE-SEM, JEOL 1350).

Electrochemical measurements.—Electrochemical impedance spectroscopy (EIS) measurements in a synthetic air flux at temperatures from 200 to 600°C were performed with a frequency response analyzer (FRA, Solartron 1255) connected via a general purpose interface bus (GPIB) to a dielectric interface (Solartron 1296) and a personal computer. The samples were placed into a quartz chamber

* Electrochemical Society Active Member.
** Electrochemical Society Student Member.
z E-mail: traversa@uniroma2.it

11 505

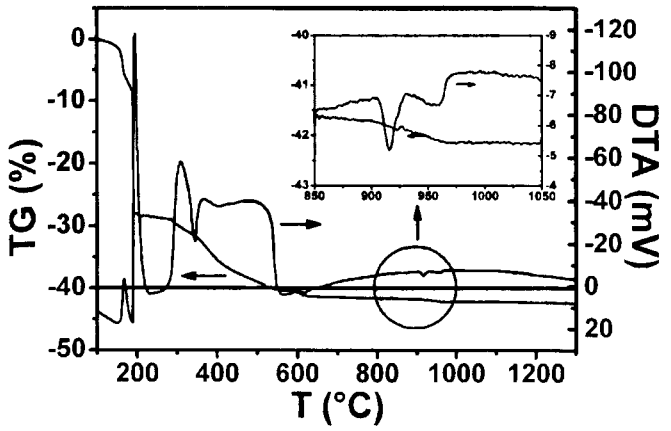

Figure 1. TG/DTA curves of the perovskite precursor dried at 100°C.

and positioned inside a tubular furnace. Gold wires connected the specimen electrode surfaces to FRA cables. EIS measurements at 600°C over an oxygen partial pressure ranging from 10^{-5} to 1 atm were carried out using a FRA (Solartron 1260) connected via GPIB to a personal computer. All measurements were performed in the 10 MHz-10 mHz frequency range. The amplitude of the applied voltage signal was 100 mV. EIS data were analyzed using Z-view software. Details of the experimental setup are described elsewhere.[10]

Results and Discussion

Powder characterization.—Figure 1 shows the TG-DTA curves of the precursor gel dried at 100°C. The total weight loss from room temperature to 1400°C was 43 wt %. A weight loss of about 28 wt % was observed up to 200°C, accompanied by two sharp exothermic peaks, which can be attributed to the decomposition of the precursor (exothermic and endothermic processes) and subsequent combustion of organic components (exothermic processes). Between 300 and 600°C, a further weight loss accompanied by broad exothermic effects was observed, also due to combustion of organic residues. The TG curve showed an additional weight loss of about 2 wt % accompanied by an endothermic peak with its maximum at about 920°C (inset, Fig. 1). The weight remained constant above 950°C.

To clarify the thermal effects observed above 200°C, a sample of the precursor gel dried at 100°C was fired at 200°C for 15 h. Figure 2 shows the TG-DTA curves of this sample. In this case, the total weight loss was approximately 15 wt % and started at about 350°C. The exothermic combustion in air of the dried polyester (water- and glycol-free) showed two different weight loss steps, accompanied by

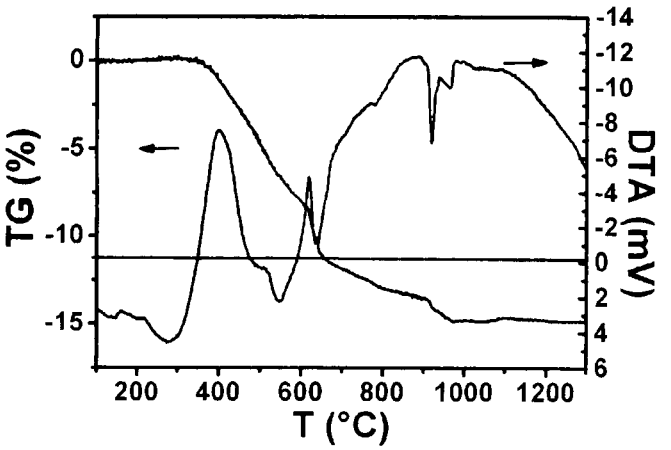

Figure 2. TG/DTA curves of the perovskite precursor dried at 100°C and then fired at 200°C for 15 h.

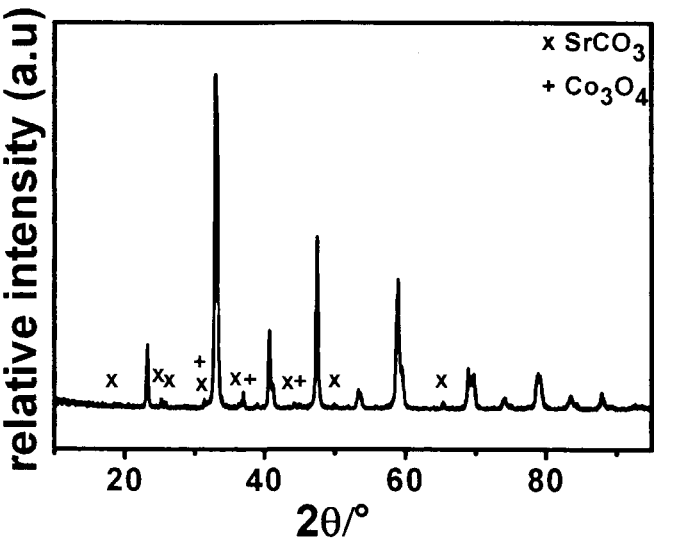

Figure 3. XRD pattern of the perovskite powder calcined at 800°C for 1 h. The unmarked peaks correspond to the $La_{0.8}Sr_{0.2}Co_{0.8}Fe_{0.2}O_{3-\delta}$ structure.

two exothermic peaks with their maxima at 400 and at 617°C. A weight loss of 1.2 wt % was observed in the temperature range 900-960°C, accompanied by two endothermic peaks with their minima at 910 and 960°C, showing that the decomposition process occurs in two steps. No weight loss was observed above 960°C.

X-ray diffraction (XRD) analysis was performed to elucidate the endothermic decomposition process at about 950°C. Figure 3 shows the XRD pattern of the $La_{0.8}Sr_{0.2}Co_{0.8}Fe_{0.2}O_{3-\delta}$ powder calcined at 800°C for 1 h. Apart from the peaks of the perovskite-type structures, $SrCO_3$ and Co_3O_4 phases were detected as impurities.

Figure 4 shows the XRD pattern of the $La_{0.8}Sr_{0.2}Co_{0.8}Fe_{0.2}O_{3-\delta}$ powder fired at 1100°C for 1 h. The thermal treatment at 1100°C left only the Co_3O_4 phase detectable as an impurity, in addition to the perovskite peaks.

Therefore, the endothermic weight loss should be ascribed to the complete decomposition of $SrCO_3$. The presence of a small amount of $SrCO_3$ in the perovskite-type oxide powders calcined at 800°C should be due to the reaction between SrO, formed from the nitrate decomposition, and CO_2, produced from combustion processes.

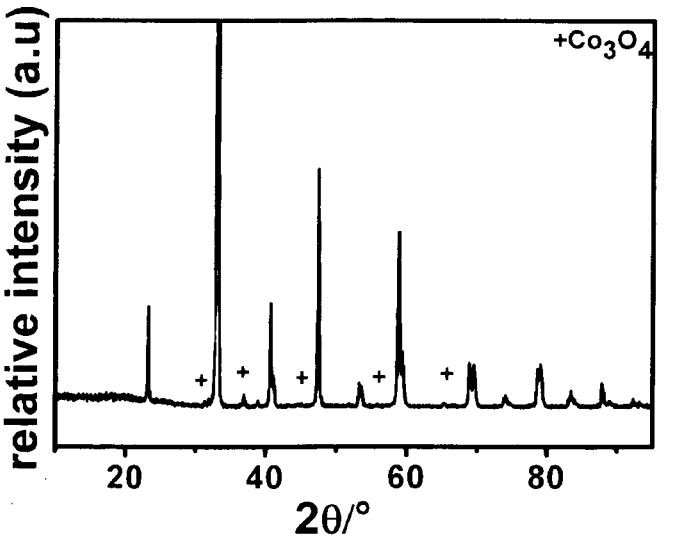

Figure 4. XRD pattern of the perovskite powder calcined at 1100°C for 1 h. The unmarked peaks correspond to the $La_{0.8}Sr_{0.2}Co_{0.8}Fe_{0.2}O_{3-\delta}$ structure.

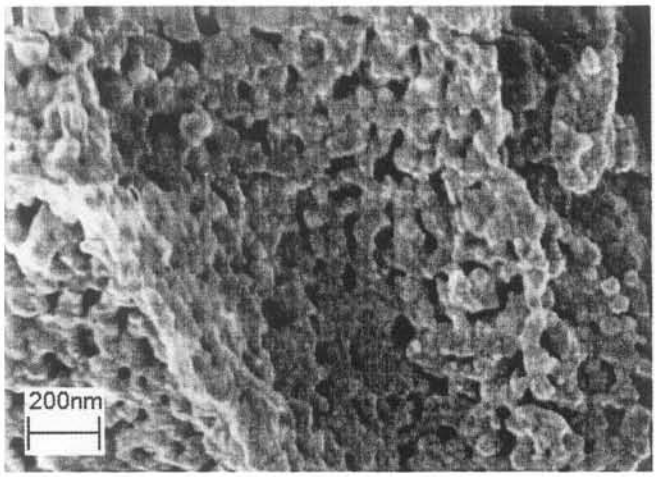

Figure 5. FE-SEM micrograph of the LSCF thick film sintered at 800°C for 1 h.

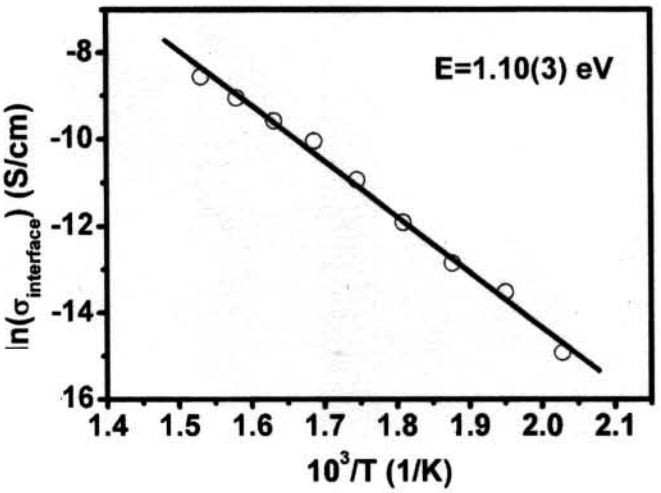

Figure 7. Arrhenius plot of the interfacial conductivity in a LSCF/YSZ/LSCF cell.

This is a common feature in the amorphous gel process when polyfunctional organic acids are used as gelling agents. The amorphous citrate processes can also lead to the presence of residual carbon after the precursor decomposition/oxidation.[11]

On the other hand, the presence of cobalt oxide as an impurity has been also reported previously by other authors; Tai *et al.*[12] observed traces of cobalt oxide in as-calcined $La_{0.8}Sr_{0.2}Co_{1-y}Fe_yO_{3-\delta}$ powders with $y \leq 0.2$, though with slight influence on the electrical properties. Electrochemical properties of perovskite-type oxides can be strongly affected by stoichiometric deviation of dopant elements and segregation of resistive phases at grain boundaries. $Ln_{0.8}Sr_{0.2}Co_{0.8}Fe_{0.2}O_{3-\delta}$ (Ln = La, Pr, Nd, Sm, Eu, Gd) powders prepared by amorphous citrate synthesis showed the presence of cobalt oxide and some evidence for phase impurities for all perovskites of rare-earth elements involved.[13] Small stoichiometric deviations of strontium and/or iron content in $La_{0.8}Sr_{0.2}Co_{0.8}Fe_{0.2}O_{3-\delta}$ due to cobalt oxide segregation could lead to the formation of the rhombohedral structure rather than the desirable orthorhombic phase, with a slight variation of the electrical properties of the perovskite material.[12]

Film characterization.—Given the combined results of TG-DTA and XRD analyses, showing that the powder calcined at 1100°C was made nearly entirely of LSCF single-phase, the films for electrochemical characterization were prepared by depositing by wet spraying the LSCF powder calcined at 1100°C on both sides of the tape cast yttria stabilized zirconia (YSZ).

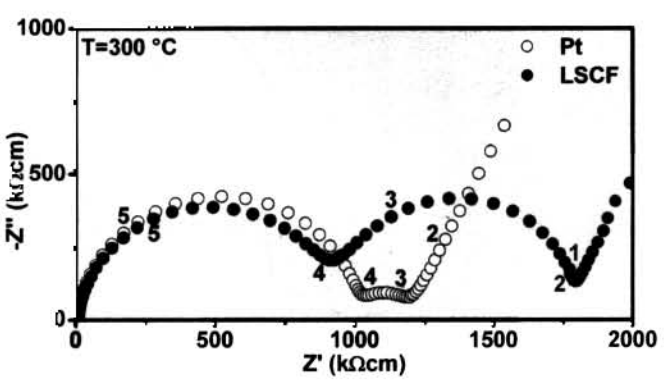

Figure 6. Impedance diagrams of Pt/YZS/Pt (open circles) and LSCF/YSZ/LSCF (closed circles) measured at 300°C. The numbers stand for the frequency logarithm.

It has been reported that LSCF cannot be applied for SOFC at high temperature (1000°C) because it reacts with YSZ.[14] Therefore, the fabrication of the films was performed at 800°C to avoid the formation of third phases at the LSCF/YSZ interface and/or decomposition of the perovskite-type oxide. For the same reason, the electrochemical characterization was performed at a temperature not exceeding 600°C.

Figure 5 shows the FE-SEM micrograph of the LSCF thick film sintered at 800°C for 1 h. The microstructure obtained is very promising, a highly porous structure made of partially sintered perovskite-type particles with grain size between 20 and 100 nm. Therefore, the specific surface area of this film is very high, which is extremely desirable for improving the cathode performance in a SOFC.[4]

Figure 6 shows the impedance spectra of Pt/YSZ/Pt and LSCF/YSZ/LSCF electrochemical cells measured under synthetic air at 300°C. The choice to study cells with symmetrical electrodes was made to unambiguously evaluate the electrochemical characterization of the specific LSCF/YSZ interface. As it is well known, the electrolyte and electrode polarization resistances are dramatically influenced by the electrolyte and electrode materials used in each cell, and by their interaction.[15] At relatively low temperatures, approximately 400°C, the impedance response of a cell using YSZ as the electrolyte is characterized by two well-defined depressed semicircles that are correlated with the contributions of bulk, in the high frequency (HF) domain, and grain boundary, in the intermediate frequency (IF) domain. At lower frequencies the response is due to electrode polarization.[16] The complex impedance diagrams shown in Fig. 6 show these three different contributions to the total electrical resistance. Moreover, Fig. 6 shows that the HF semicircle remained almost unchanged when Pt or LSCF electrodes were used. On the other hand, a large difference was observed in the IF semicircles of the Pt/YSZ/Pt and LSCF/YSZ/LSCF specimens, showing an increase in the electrical resistance with LSCF electrodes. This resistance may be enlarged by interfacial phenomena, like constriction resistance attributed mainly to blocking regions in the electrolyte/electrode interface and/or high resistive phase(s) at this interface.[17] As shown also by Tu *et al.*,[18] at sintering temperatures of 800°C insulating phases are not formed at the LSCF/YSZ interface. Therefore, the increase in the resistance at intermediate frequencies reported here cannot be ascribed to the formation of resistive phases formed by a chemical reaction at the LSCF/YSZ interface. The separation of the effects occurring in the intermediate frequency range is difficult by conventional fitting since the time constants involved are too close.

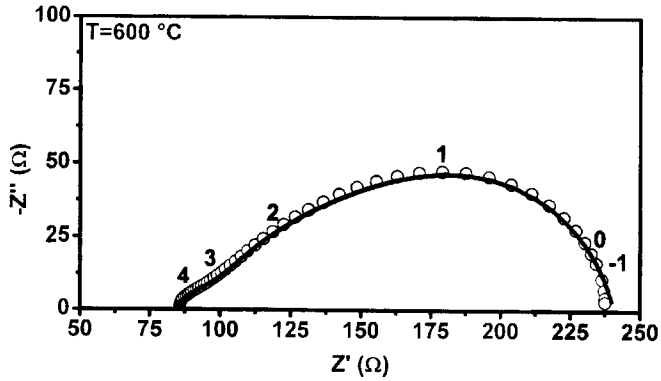

Figure 8. Typical impedance diagram of a LSCF/YSZ/LSCF cell, showing the experimental and the fitted data. The numbers stand for the frequency logarithm.

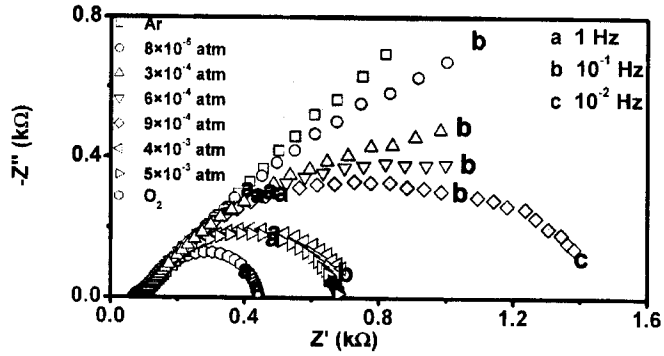

Figure 10. Impedance diagrams of a LSCF/YSZ/LSCF cell under different oxygen partial pressures (measured at 600°C).

This additional interface contribution in the LSCF/YSZ/LSCF cell can be estimated by the frequency subtraction of both LSCF/YSZ/LSCF and Pt/YSZ/Pt impedance diagrams. This procedure was followed to evaluate the data plotted in Fig. 7, which shows the temperature dependence of the interfacial conductivity ($\sigma_{interface}$). The activation energy from the Arrhenius plot is 1.10(3) eV. Such a value is very close to the activation energy for ion oxide migration at grain boundaries in YSZ. Moreover, this additional contribution in the intermediate frequency range presents a mean capacitance value of approximately 10^{-11} F and could be attributed to the LSCF bulk contribution to the total ionic conductivity of the cell.

Figure 8 shows a typical impedance diagram obtained for the LSCF/YSZ/LSCF cell at 600°C under dynamic synthetic air. In this electrode frequency domain two decentralized semicircles can be separated and fitted by two R//C in series. The semicircles' depression is usually expressed by decentralization angles. These semicircles can be ascribed to different processes that determine the polarization resistance of the cathode in a SOFC.

Figure 9 shows the temperature dependence of the area specific resistance (ASR) and activation energies for both intermediate frequency (IF) and low frequency (LF) processes. The ASR was determined by the product of the electrode resistance to the electrode area values.

The activation energy of the IF process was determined to be 1.11(7) eV (Fig. 9) and could be related to the ionic conduction in the LSCF electrodes. The activation energy of the LF process was determined to be 1.62(3) eV (Fig. 9), indicating that the mechanism leading to the detection of the semicircle at low frequencies yields a limitation step to the reaction rates and charge transfer at these electrodes. To identify this limiting reaction, EIS measurements were performed over a range of different oxygen partial pressures. Figure 10 shows the impedance diagrams for the LSCF/YSZ/LSCF cell measured at 600°C under different oxygen partial pressures. The evolution of the semicircle at LF shows that it increases for decreasing oxygen partial pressure, thereby resulting in an increase of the electrical resistance for decreasing p_{O_2}.

Figure 11 shows the dependence of the ASR for the low-frequency semicircle on the oxygen partial pressure, evaluated from the data reported in Fig. 10. Such dependence, $(p_{O_2})^{1/2}$, indicates that the rate-limiting step for the LSCF electrode reaction is an adsorption/desorption mechanism with associated activation energy of approximately 1.6 eV in the low oxygen partial pressure region.[19,20]

Conclusions

The interface between MIEC used as electrode in a system with a pure ionic conductor as the electrolyte was successfully studied by electrochemical impedance spectroscopy. The spray technique was successfully used to produce a porous cathode material, which is extremely desirable for improving the cathode performance in a

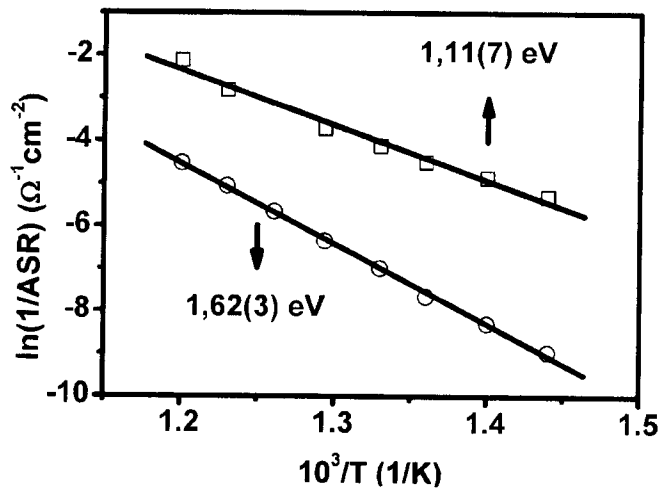

Figure 9. Temperature dependence of the ASR and activation energies for each electrode process in the LSCF/YSZ/LSCF cell. The squares and circles represent the ASR values calculated from the intermediate and low frequency semicircles in the impedance diagrams, respectively.

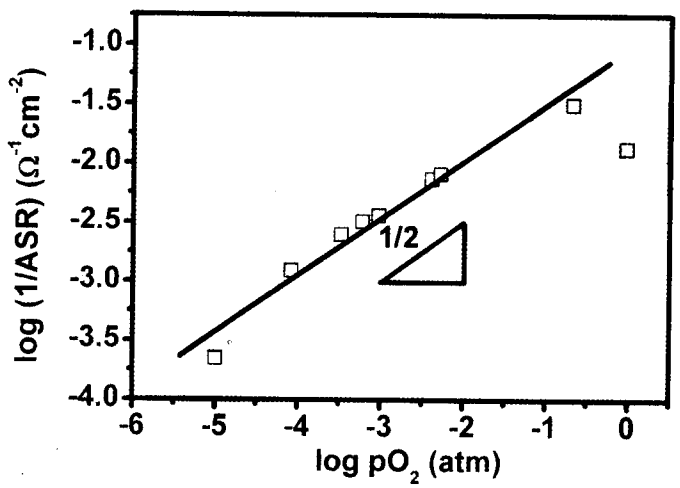

Figure 11. Log-log plot of the dependence on the oxygen partial pressure of the reciprocal of ASR of the limiting step in the electrode reaction (LF semicircle in the impedance diagram, see Fig. 8).

SOFC. The limiting process in LSCF/YSZ/LSCF cells was found to be a adsorption/desorption reaction with an activation energy of approximately 1.6 eV.

Acknowledgements

This work was partly supported by the Italian Ministry of Education, University and Research (MIUR) and FAPESP-S. Paulo, Brazil (Process 99/10798-0). One of the authors (D.Z.F.) acknowledges CAPES Foundation (Brazil) for the scholarship (BEX2187/01-9).

References

1. N. Minh, *J. Am. Ceram. Soc.*, **76**, 563 (1993).
2. J. W. Yoon, M. L. Grilli, E. Di Bartolomeo, R. Polini, and E. Traversa, *Sens. Actuators B* , **76**, 483 (2001); M. L. Grilli, E. Di Bartolomeo, and E. Traversa, *J. Electrochem. Soc.*, **148**, H98 (2001); E. Di Bartolomeo, N. Kaabbuathong, A. D'Epifanio, M. L. Grilli, E. Traversa, H. Aono, and Y. Sadaoka, *J. Eur. Ceram. Soc.*, In press.
3. S. P. Jiang, *Solid State Ionics*, **146**, 1 (2002).
4. V. Dusastre and J. A. Kilner, *Solid State Ionics*, **126**, 163 (1999).
5. A. J. McEvoy, *Solid State Ionics*, **132**, 159 (2000).
6. M. P. Pechini, U.S. Pat. 3,330,697 (1967).
7. D. Stöver, P. Buchkremer, F. Tietz, and N. H. Menzler, in *5th European Solid Oxide Fuel Cell Forum*, Proc. Vol. 1, J. Huijsmans, Editor, p. 1, Lucerne, Switzerland, European Fuel Cell Forum (2002).
8. E. Spila, S. Panero, and B. Scrosati, *Electrochim. Acta*, **43**, 1651 (1998).
9. M. M. da Vila, M. P. Elizalde, and R. Silva, *J. Mater. Sci.*, **32**, 3705 (1997).
10. M. C. Steil, F. C. Fonseca, Y. V. França, J. F. Q. Rey, E. N. S. Muccillo, and R. Muccillo, *Cerâmica*, **48**, 146 (2002).
11. M. S. G. Baythoun and F. R. Sale, *J. Mater. Sci.*, **17**, 2757 (1982).
12. L. W. Tai, M. M. Nasrallah, H. U. Anderson, D. M. Sparlin, and S. R. Sehlin, *Surf. Sci. Lett.*, **76**, 250 (1995).
13. F. Riza, Ch. Ftikos, F. Tietz, and W. Fischer, *J. Eur. Ceram. Soc.*, **21**, 1769 (1995).
14. O. Yamamoto, Y. Takeda, R. Kanno, and M. Noda, *Solid State Ionics*, **22**, 241 (1987).
15. M. Liu and Z. Wu, *Solid State Ionics*, **107**, 105 (1998).
16. M. Kleitz, H. Bernard, E. Fernandez, and E. Schouler, in *Science and Technology of Zirconia, Advances in Ceramics*, Vol. 3, A. H. Heuer and L. W. Hobbs, Editors, p. 310. The American Ceramic Society Inc., Columbus, OH (1981).
17. S. B. Adler, *Solid State Ionics*, **111**, 125 (1998).
18. H. Y. Tu, Y. Takeda, N. Imanishi, and O. Yamamoto, *Solid State Ionics*, **117**, 277 (1999).
19. A. Ringuedé and J. Fouletier, *Solid State Ionics*, **139**, 167 (2001).
20. M. Koyama, C.-Ju. Wen, T. Masuyama, J. Otomo, H. Fukunaga, K. Yamada, K. Eguchi, and H. Takahashi, *J. Electrochem. Soc.*, **148**, A795 (2001).